Title

Statistical mechanical model of gas adsorption in porous crystals with dynamic moieties

Journal

Proceedings of the National Academy of Sciences of the United States of America, 114(3)

ISSN

0027-8424

Authors

Simon, Cory M
Braun, Efrem
Carraro, Carlo
et al.

Publication Date

2017-01-17

DOI

10.1073/pnas.1613874114

Peer reviewed

Statistical mechanical model of gas adsorption in porous crystals with dynamic moieties

Cory M. Simon[a], Efrem Braun[a], Carlo Carraro[a,1], and Berend Smit[a,b,1]

[a]Department of Chemical and Biomolecular Engineering, University of California, Berkeley, CA 94709; and [b]Laboratory of Molecular Simulation, Institut des Sciences et Ingénierie Chimiques, Valais Ecole Polytechnique Fédérale de Lausanne (EPFL), CH-1951 Sion, Switzerland

Edited by David Jenkins, University of Tennessee, and accepted by Editorial Board Member John D. Weeks November 23, 2016 (received for review August 19, 2016)

Some nanoporous, crystalline materials possess dynamic constituents, for example, rotatable moieties. These moieties can undergo a conformation change in response to the adsorption of guest molecules, which qualitatively impacts adsorption behavior. We pose and solve a statistical mechanical model of gas adsorption in a porous crystal whose cages share a common ligand that can adopt two distinct rotational conformations. Guest molecules incentivize the ligands to adopt a different rotational configuration than maintained in the empty host. Our model captures inflections, steps, and hysteresis that can arise in the adsorption isotherm as a signature of the rotating ligands. The insights disclosed by our simple model contribute a more intimate understanding of the response and consequence of rotating ligands integrated into porous materials to harness them for gas storage and separations, chemical sensing, drug delivery, catalysis, and nanoscale devices. Particularly, our model reveals design strategies to exploit these moving constituents and engineer improved adsorbents with intrinsic thermal management for pressure-swing adsorption processes.

metal–organic frameworks | flexible metal–organic frameworks | statistical mechanics | porous materials | gas storage

Metal–organic frameworks (MOFs) are porous, crystalline materials with very large internal surface areas (1). The consequent adsorption properties of MOFs have demonstrated promise toward solving paramount energy problems (2) such as in gas storage (3) and gas separations (4). MOFs are also being explored for chemical sensing (5), drug delivery (6), and catalysis (7). In the synthesis of MOFs, metal nodes or clusters and organic linker molecules self-assemble (8). Owing to their modular and versatile chemistry, tens of thousands of MOFs have been synthesized (9).

Some MOFs are dynamic/flexible and respond to gas molecules adsorbing into their pores by exhibiting structural changes while retaining their crystallinity (reviews in refs. 10–14). Reported modes of guest-induced structural changes in MOFs include breathing (15), swelling (16), and subnetwork displacement (17), as well as less dramatic changes, such as the rotation of a ligand (18) or deformation (19). In molecular recognition and enzyme catalysis in biology, a conformation change of the enzyme is often involved in substrate binding (20, 21). Responsive, dynamic constituents thus may endow MOFs with enzyme-like selectivities (11) for selective gas adsorption, chemical sensing, and catalysis.

In the long run, a more intimate understanding of MOFs with moving parts may enable the construction of molecular machines (22). Because of their crystallinity and tunability, MOFs are an ideal scaffold on which to organize machine subunits and tune their response to stimuli. Notably, Zhu et al. (23) used a [2] rotaxane molecular switch as a building block in a MOF to construct a conceptual molecular machine.

Several reported MOFs possess dynamic constituents, e.g., bridging ligands that can rotate, while maintaining an approximately rigid unit cell (18, 24–28, 28–34). Nuclear magnetic resonance (NMR) spectroscopy revealed that aromatic rings in the ligands of MOF-5 (26), IRMOF-3 (27), and MIL-47(V) (35) rotate, resembling an ordered assembly of molecular rotors (36). Horike et al. (24) synthesized MOFs with rotating pyrazine and naphthalene rings and found that the naphthalene rings can adopt one of four distinct rotational conformations. Murdock et al. (37) synthesized a 2D MOF whose sheets stack to construct one-dimensional tube architectures; depending on the guest molecules, a phenyl ring in the linker can protrude into the channel or align with the channel walls, modulating the diameter of the channel. Subsequently, Hughes et al. (38) synthesized a series of MOFs isoreticular to this 2D MOF with rotating aryl rings in differing pore sizes.

When the dominant conformations of these flexible parts in MOFs are different in the evacuated solid than in the presence of gas, the dynamic moieties can qualitatively affect the adsorption behavior, e.g., by inducing inflections (30), steps (29), and hysteresis (18) in the adsorption isotherms. Linkers in ZIF-7 are believed to rotate and cause steps and hysteresis in the adsorption isotherms of several hydrocarbons (39, 40). Ligands in a MOF in ref. 18 were shown to rotate upon CO_2 adsorption to accommodate more molecules, leading to an inflection and hysteresis in the CO_2 adsorption isotherm. Seo et al. (29) engineered a framework with rotating pillars bearing side chains that reach across a cage to lock together, serving as a molecular gate. When immersed in a bath of CO_2 gas, the locks

Significance

Some nanoporous, crystalline materials possess dynamic/flexible constituents, for example, a ligand that can rotate. Much like the induced-fit model of enzyme–substrate binding in biology, these dynamic moieties often change conformation when gas molecules adsorb. Such flexible constituents may endow nanoporous materials with enhanced properties for gas storage and separations, chemical sensing, drug delivery, and catalysis. We developed and solved a statistical mechanical model of gas adsorption in a porous material with a rotating ligand that is shared between cages. Our model contributes a more intimate understanding of gas adsorption in nanoporous materials with moving parts and lends insights into how to harness these dynamic constituents for adsorption-based processes.

Author contributions: C.M.S., E.B., C.C., and B.S. designed research; C.M.S. and E.B. performed research; and C.M.S., E.B., C.C., and B.S. wrote the paper.

The authors declare no conflict of interest.

This article is a PNAS Direct Submission. D.J. is a Guest Editor invited by the Editorial Board.

Freely available online through the PNAS open access option.

Data deposition: The codes used to produce the plots in this paper are included on Github at doi.org/10.5281/zenodo.208230.

[1]To whom correspondence may be addressed. Email: carraro@berkeley.edu or Berend-Smit@Berkeley.edu.

This article contains supporting information online at www.pnas.org/lookup/suppl/doi:10.1073/pnas.1613874114/-/DCSupplemental.

between these rotating pillars break to increase the porosity. A signature of the rotating pillars was revealed in the CO_2 adsorption isotherm through steps and hysteresis. The ligands in MIL-91(Al) undergo a twist upon CO_2 adsorption (30); similarly to the case in ref. 18, an inflection point in the CO_2 adsorption isotherm was observed as a consequence of the ligand rotation, but no hysteresis was observed. Uemura et al. (41) reported a MOF whose aromatic rings rotate upon the adsorption of isopropanol. Recently, Krause et al. (42) reported a negative gas adsorption step in DUT-49 as a result of a conformation change in its ligand and the consequent change in pore size. Hyun et al. (43) reported a MOF whose ligands possess two propyl side groups that block the pores. When immersed in CO_2 gas, the ligands rotate, opening the pore and giving rise to an abrupt step in the adsorption isotherms.

A greater understanding of the thermodynamics of adsorption in MOFs with dynamic moieties can facilitate their design to harness them for chemical sensing, gas storage and separations, catalysis, drug delivery, and the construction of molecular machines. For example, for pressure-swing adsorption processes, there is significant value in engineering MOFs with ligands that undergo a conformation change upon gas adsorption. First, their S-shaped gas adsorption isotherms enhance the attainable working capacity compared with a rigid material; if the operating pressures bracket the inflection point/step, a MOF with a rotating ligand can achieve higher (lower) uptake at the high (low) pressure than an optimally shaped (44, 45) Langmuir adsorption isotherm. Second, as the ligands prefer a different conformation in the absence of gas, the ligand conformation change is endothermic; the ligand rotations consequently consume (provide) some of the heat released (consumed) upon adsorption (desorption). Such intrinsic heat management mitigates working capacity losses during the pressure swing that arise due to temperature changes of the adsorbent (46).

Simple thermodynamic models of adsorption, e.g., the Langmuir and Brunauer–Emmett–Teller (BET) models, have proved useful for understanding adsorption phenomena, interpreting experimental data, and designing adsorption-based engineering processes. Analytical models of adsorption in breathing and gate-opening MOFs have been developed (47–50); these models characterize the state of the framework with a scalar order parameter α and prescribe the free energy of the host as a function of α. Dunne and Manos (51) took a different approach and defined four characteristic states of the unit cell of a breathing MOF and prescribed the neighboring interaction between them.

To obtain fundamental insights into how ligand rotations influence adsorption behavior, we build and solve a statistical mechanical model of gas adsorption in a porous crystal whose cages share a rotatable moiety. The moiety in the empty host has a preference for a particular rotational conformation. Adsorbed guest molecules, however, have a greater affinity for the ligand in a different rotational conformation. Thus, in opposition to intrahost forces, adsorbed gas incentivizes the moieties to adopt a different rotational conformation than in the evacuated host. Our model captures inflections, steps, and hysteresis in the adsorption isotherm that can arise as a consequence of the dynamic moieties that we show are effectively a source for cooperative adsorption.

Model Description

Fig. 1 depicts our model porous crystal with rotatable ligands/moieties. The model material consists of M cages that can each adsorb at most a single gas molecule. Each ligand is shared by two cages and adopts one of two states: parallel to the cage walls or rotated into the pore. The character of the model arises from the host and guest molecule having opposite energetic preferences

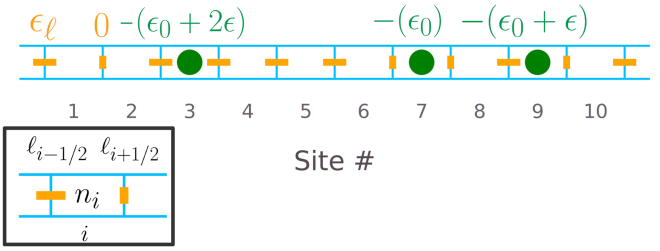

Fig. 1. Quasi–one-dimensional model porous material with rotating moieties. Each blue rectangle represents one of M adsorption cages ($M = 10$ here). The green ball represents an adsorbed gas molecule. The orange bars represent ligands that can adopt one of two conformations: rotated into the pore or parallel to the cage walls. The energies of the first two ligands are written in orange. The energy of adsorption of a gas molecule depends on the state of the ligand to the left and right of it. Written in green are energies experienced by each gas molecule here. *Inset* showing a general cage i illustrates our variable convention. For example, $n_1 = 0$, $n_3 = 1$, $\ell_{1/2} = 1$, and $\ell_{3/2} = 0$ here.

for the rotational conformation of the ligand: Intrahost forces impose an energetic penalty ϵ_ℓ if the ligand is rotated into the pores; on the other hand, a guest molecule has a higher affinity for the ligand when it is rotated into the pore. The energy of an adsorbed guest molecule inside a cage when ligands on both sides are parallel to the cage walls is $-\epsilon_0$. The electrostatic and/or van der Waals interactions between a guest molecule and a ligand are enhanced by an energy $-\epsilon$ when a ligand is rotated into the pores. Fig. 1 depicts the three distinct environments and associated energies encountered by an adsorbed guest molecule. Note that adsorbed gas molecules here do not directly interact except through volume exclusion by enforcing at most one adsorbate per cage.

We now write an expression for the internal energy of our system, defined as the model material with M cages and n adsorbed guest molecules as in Fig. 1. Let n_i be the occupancy state of cage i; $n_i = 1$ if the cage is occupied with a guest molecule and $n_i = 0$ if it is empty. Let $\ell_{i+1/2}$ be the state of the ligand on the right face of cage i; $\ell_{i+1/2} = 0$ if the ligand is aligned with the pore walls and $\ell_{i+1/2} = 1$ if it is rotated into the pores. Fig. 1 and Table 1 summarize our variable convention. We impose periodic boundary conditions to mimic an infinite crystal by enforcing $\ell_{i+1/2} = \ell_{i+1/2+M}$ and $n_i = n_{i+M}\ \forall\, i \in \mathbb{Z}$, effectively folding the lattice into a ring. A microstate of our system is characterized by the M-dimensional vectors $\mathbf{n}$ and $\boldsymbol{\ell}$, whose ith component is n_i and $\ell_{i-1/2}$, respectively. The internal energy U of the system for a given microstate is then

$$U(\mathbf{n},\boldsymbol{\ell}) = \epsilon_\ell \sum_{i=1}^{M} \ell_{i-1/2} - \sum_{i=1}^{M} n_i(\epsilon_0 + (\ell_{i-1/2} + \ell_{i+1/2})\epsilon). \quad \textbf{[1]}$$

The first term is the intrahost energy. The second term is the energy of the adsorbed guest molecules, which depends on the states of the ligands. The intriguing question is how the two competing preferences in Eq. **1** will play out: The host prefers the ligands to remain parallel to the cage walls whereas adsorbed guest molecules incentivize the ligands to rotate into the pores.

We consider our model porous material in the grand-canonical (μVT) ensemble, where the adsorbed phase of guest molecules in the material is in thermodynamic equilibrium with a bath of bulk gas with fixed chemical potential μ and inverse thermodynamic temperature $\beta := 1/(k_B T)$. Here, M plays the role of volume; a guest molecule has access to a free volume V_0 in each adsorption cage. The grand-canonical ensemble corresponds to experimental measurements of the equilibrium gas adsorption isotherm in a porous material. The chemical

Table 1. Model parameters and variables

Parameters	Description
M	No. of adsorption cages
V_0	Free volume for adsorbate in each cage
ϵ_ℓ	Intrahost energetic penalty for ligand rotation
$-\epsilon_0$	Energy of adsorbate in cage with both ligands aligned with cage walls
$-\epsilon$	Enhancement of guest–ligand interaction when ligand is rotated into the cage
$\ell_{i+1/2}$	Rotational state of ligand on right face of cage i (0, parallel to cage wall; 1, rotated into pores)
n_i	Occupancy state of adsorption cage i (0, empty; 1, occupied)
$\ell := \sum \ell_{i+1/2}$	No. of ligands rotated into the pores
$n := \sum n_i$	No. of adsorbed guest molecules

potential is related to the pressure of the bulk gas through an equation of state, such as the ideal gas law we apply here. Our first objective is to find common experimental measurables in our model, including the gas adsorption isotherm and isosteric heat of adsorption.

Results

It is instructive to first examine two extreme cases: (*i*) $\epsilon_\ell \to \infty$, where all ligands are aligned with the cage walls, and (*ii*) $\epsilon_\ell \to -\infty$, where all ligands are rotated into the pores. Both cases result in a nondynamic/rigid porous material with a Langmuir adsorption isotherm

$$\langle n_i \rangle = \frac{KP}{1+KP}, \qquad [2]$$

where P is the pressure of the bulk gas in equilibrium with the adsorbed phase in the material and K is the Langmuir constant representing the affinity of the gas molecule for the walls of the pores. The model material in case *i* (*ii*) exhibits a Langmuir constant $K_1 = \beta V_0 e^{\beta\epsilon_0}$ ($K_2 = \beta V_0 e^{\beta(\epsilon_0+2\epsilon)}$) (45) because an adsorbed guest molecule would invariably experience an energy of adsorption ϵ_0 ($\epsilon_0 + 2\epsilon$). The Langmuir adsorption isotherms in these two extreme cases are depicted in Fig. 2, *Left* as the blue and red curves. The adsorption isotherm in case *ii* saturates at a lower pressure as a result of the greater affinity of a gas molecule for the host when the ligands are rotated into the pores. In both cases, the number of adsorbed molecules approaches the number of adsorption cages, M, as $P \to \infty$.

The adsorption isotherm in our model material must then lie between the two extreme curves in Fig. 2. Although not rigorous, it is helpful to interpret our model material as transitioning between two states as it adsorbs gas. When the host is empty, the majority of the ligands are aligned with the cage walls if $\beta\epsilon_\ell$ is appreciably large. Consequently, the gas sees an adsorbent more like case *i* at low pressures. When filled with gas, the energy of the system is minimized when the ligands rotate into the pores if $2\epsilon/\epsilon_\ell$ is sufficiently large. Consequently, the adsorbent looks like case *ii* at higher pressures. For a subset of parameter space, the adsorption isotherm in our model passes through an inflection as the host transitions from approximately the material in case *i* to approximately the material in case *ii*, as shown in the green curve in Fig. 2 that is an example adsorption isotherm in our model that we derive below. In reality, the adsorbed gas gradually changes the set of most probable conformations that the host adopts (i.e., this is not a two-state model).

A transitioning of the host from one state to another as it adsorbs gas, however, does not necessitate the presence of an inflection in the adsorption isotherm. We later show that the convexity at low pressures in our model arises through cooperative adsorption: When an adsorbed gas molecule induces a neighboring ligand to rotate into the pores, it creates a more favorable binding site in the neighboring cage, facilitating the recruitment of an additional guest molecule (if that neighboring cage is empty). The adsorption curve then switches to be concave as the cages saturate with guest molecules.

The Partition Function. The grand-canonical partition function Ξ of the model in Fig. 1 is a sum over all microstates $\mathbf{n}$ and $\boldsymbol{\ell}$,

$$\Xi(\mu, M, \beta) = \sum_{\mathbf{n}} \sum_{\boldsymbol{\ell}} \left(V_0 \Lambda^{-3}\right)^n e^{\beta\mu n - \beta U(\mathbf{n},\boldsymbol{\ell})}, \qquad [3]$$

with the internal energy $U(\mathbf{n}, \boldsymbol{\ell})$ given in Eq. **1**. The $V_0\Lambda^{-3}$ term arises from the configurational partition function and is related to the translational entropy of the adsorbate in the cage; Λ is the de Broglie wavelength of the guest molecule.

We can explicitly evaluate the sum over $\boldsymbol{\ell}$ in Eq. **3**, effectively resulting in a coupling of the occupancy of neighboring cages through their shared ligand. We then perform the sum over $\mathbf{n}$, using the transfer-matrix method. See *SI Appendix*, section S1 for an expanded derivation. We define a 2×2 transfer matrix $\mathbf{P}$ that enumerates the statistical weights in the partition function for the four possible values of (n_{i-1}, n_i):

$$\mathbf{P} := \begin{bmatrix} 1 + e^{-\beta\epsilon_\ell} & (1 + e^{\beta(\epsilon-\epsilon_\ell)})\sqrt{\Lambda^{-3} V_0 e^{\beta(\mu+\epsilon_0)}} \\ (1 + e^{\beta(\epsilon-\epsilon_\ell)})\sqrt{\Lambda^{-3} V_0 e^{\beta(\mu+\epsilon_0)}} & \Lambda^{-3} V_0 e^{\beta(\mu+\epsilon_0)}(1 + e^{\beta(2\epsilon-\epsilon_\ell)}) \end{bmatrix}. \qquad [4]$$

Our transfer matrix $\mathbf{P}$ is symmetric positive definite for $\epsilon \neq 0$. Therefore, it has positive eigenvalues. When $\epsilon \neq 0$, we can write

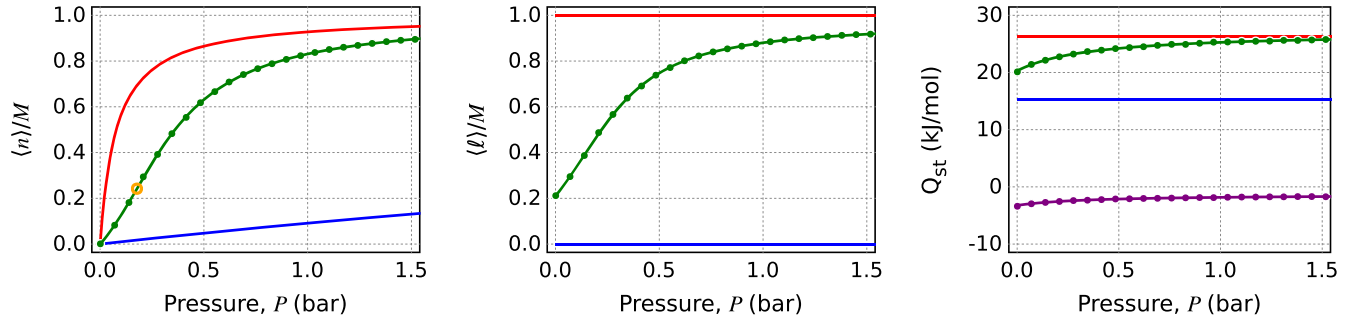

Fig. 2. Example model solution as a function of pressure. Green curve is exact model solution. Blue and red curves correspond to $\epsilon_\ell \to \pm\infty$. (*Left*) Fractional cage occupancy. The inflection point in the adsorption isotherm is annotated with the orange circle. (*Center*) Fraction of ligands rotated into the pores. (*Right*) Isosteric heat of adsorption. Purple curve is intrahost contribution. Points are from Monte Carlo simulations (*SI Appendix*, section S9).

Ξ in terms of the dominant eigenvalue λ of the matrix $\mathbf{P}$ when M is large:

$$\Xi = \lambda^M. \quad [5]$$

In *SI Appendix*, section S1.1, we show that we recover the partition function of a Langmuir model with energy of adsorption ϵ_0 ($\epsilon_0 + 2\epsilon$) when $\epsilon_\ell \to \infty$ ($\epsilon_\ell \to -\infty$), confirming our claims that Eq. **2** governs the adsorption in the limits $\epsilon_\ell \to \pm\infty$.

Relating Model to Experiments. Here, we relate our model to commonly measured experimental quantities. The chemical potential μ is imposed by the bulk gas in equilibrium with the adsorbed phase in the grand-canonical ensemble. To correspond to experiments that measure the pressure P of the gas, we replace the chemical potential μ in our model with that of an ideal gas (52):

$$\mu = k_B T \log(\beta P \Lambda^3). \quad [6]$$

In the plots that follow, we use the parameter set $\epsilon_\ell = 3$ kJ/mol, $\epsilon = 5.5$ kJ/mol, $\epsilon_0 = 13$ kJ/mol, $T = 273$ K, and $V_0 = 12.32$ Å^3 that [we later show in *Case Study: MIL-91(Al)*] governs krypton adsorption in MIL-91(Al). The green points on the plots correspond to Monte Carlo simulations to confirm our exact solution (*SI Appendix*, section S9). The codes used to produce the plots in this paper are included on Github at doi.org/10.5281/zenodo.208230.

Adsorption isotherm. The adsorption isotherm is the expectation of the number of adsorbed particles, $\langle n \rangle$, in our model material as a function of pressure, P:

$$\langle n \rangle = \sum_{\mathbf{n}} \sum_{\boldsymbol{\ell}} n \frac{(\Lambda^{-3} V_0)^n e^{\beta\mu n - \beta U(\mathbf{n},\boldsymbol{\ell})}}{\Xi} = \left(\frac{\partial \log \Xi}{\partial(\beta\mu)} \right)_{\beta, M}. \quad [7]$$

Fig. 2, *Left* shows the adsorption isotherm. For reference, the blue and red curves in each panel correspond to $\epsilon_\ell \to \pm\infty$. Remarkably, our simple model captures the inflection seen in gas adsorption isotherms in MOFs with ligands that change their rotational conformation upon gas adsorption. At low pressures, the adsorption curve is convex, indicating a cooperative adsorption effect. As the cages saturate with guest particles, the curve transitions and becomes concave, passing through an inflection point. This model, where cages are coupled in only one dimension, does not exhibit adsorption–desorption hysteresis; later in *Results* we find that adsorption–desorption hysteresis may arise if cages are coupled in multiple dimensions.

Ligand configurations. As the gas adsorption is linked to the concomitant rotational configurations of the ligands, we plot the expected number of ligands protruding into the pores,

$$\langle \ell \rangle = \sum_{\mathbf{n}} \sum_{\boldsymbol{\ell}} \ell \frac{(\Lambda^{-3} V_0)^n e^{\beta\mu n - \beta U(\mathbf{n},\boldsymbol{\ell})}}{\Xi} = -\left(\frac{\partial \log \Xi}{\partial(\beta\epsilon_\ell)} \right)_{\beta\mu,\beta,M}, \quad [8]$$

in Fig. 2, *Center*. In the empty host, $\langle \ell \rangle > 0$ as each ligand fluctuates about two energy states that differ by energy ϵ_ℓ. As a higher chemical potential drives more gas molecules to adsorb, the greater interaction of a guest with a ligand that is rotated into the pore (ϵ) induces more ligands to rotate into the cage. Note that, when the lattice is fully occupied, $\langle \ell \rangle < 1$ as each ligand fluctuates between its two rotational conformations that differ by energy $\epsilon_\ell - 2\epsilon$. The curve $\langle \ell \rangle(P)$ passes through an inflection coincident with the adsorption isotherm.

Isosteric heat of adsorption. The isosteric heat of adsorption Q_{st} is the amount of heat released upon the addition of a gas molecule. As Q_{st} determines the associated temperature change of the adsorbent upon ad-/desorption, it is a key thermodynamic variable in the design of adsorption-based processes (53). Furthermore, the loading dependence of Q_{st} often yields insights into the mechanism of adsorption and the structural characteristics of the material, e.g., adsorbate–adsorbate attractions (54), binding site preferences on heterogeneous surfaces (55), and structural transitions (56).

We obtain Q_{st} in our model by finding the negative enthalpy change of the system upon the addition of an adsorbate,

$$-Q_{st} := \langle U \rangle(\langle n \rangle + 1) - \langle U \rangle(\langle n \rangle) - k_B T, \quad [9]$$

where $k_B T$ is the work required to push a gas molecule from the adsorbed to the ideal, bulk gas phase. Approximating the energy difference as a derivative

$$\langle U \rangle(\langle n \rangle + 1) - \langle U \rangle(\langle n \rangle) \approx \frac{\partial \langle U \rangle}{\partial \langle n \rangle} = \frac{\langle Un \rangle - \langle U \rangle \langle n \rangle}{\langle n^2 \rangle - \langle n \rangle^2} \quad [10]$$

allows us to compute Q_{st} from fluctuations of the particle number and the covariance between the energy and particle number in the grand-canonical ensemble (57). For a rigid material, Q_{st} at dilute coverage is a metric for the affinity of the gas molecule for the walls of the material; e.g., in a Langmuir model with energy of adsorption $-U_0$, $Q_{st} = U_0 + k_B T$. As Eqs. **1** and **9** show, the heat of adsorption is impacted by ligands that undergo a conformation change induced by adsorbed molecules. Consider the conceptual process of adding an adsorbed molecule to site 6 in Fig. 1. Heat is released due to the energy of adsorption of this particle ($\epsilon_0 + \epsilon$). If, in addition, the newly adsorbed molecule in site 6 induces the ligand to its right to rotate into the pores, heat is (*i*) consumed by the endothermic process of the ligand's conformation change (ϵ_ℓ) and (*ii*) released due to the enhancement of the energetic interaction of guest 7 with the newly rotated ligand to its left (ϵ). The latter two subtle effects arise from the dynamic moiety in the material.

The green curve in Fig. 2, *Right* shows Q_{st} as a function of pressure. As a greater fraction of the ligands rotate into the pore to create more receptive adsorption cages, the heat of adsorption increases. The reason for the increase of Q_{st} with pressure is that, when a guest molecule adsorbs and incentivizes an adjacent ligand to rotate into the pore, if the adjacent cage is empty, this creates a more favorable adsorption site for the next guest molecule to adsorb in the adjacent cage, whereas if the adjacent cage is occupied—the more likely the case at higher coverage—the two neighboring adsorbates now cooperate in incentivizing the ligand to rotate into the pores, lowering the energy of the system due to the enhanced interaction with the two neighboring adsorbates.

Parameter Exploration. To gain a deeper intuition into how the energetic parameters (ϵ_0, ϵ, and ϵ_ℓ) and temperature affect the adsorption isotherm, isosteric heat of adsorption, and ligand configurations, we explored parameter space by varying a single parameter while holding the others fixed. We relegate the explanations of the parameter dependence of the model solution to *SI Appendix*, section S4. On Github, we provide an interactive dashboard in the Jupyter Notebook for readers to explore parameter space themselves (doi.org/10.5281/zenodo.208230).

Insights into Adsorption Cooperativity. The expected values in Fig. 2 obscure how the typically $\langle n \rangle$ occupied cages and $\langle \ell \rangle$ rotated ligands are arranged on the lattice. Neighboring adsorbates are not explicitly prescribed to interact with one another in our model. However, a coupling of the occupancy of two adjacent cages arises through their shared ligand. The covariance of the occupancy of two adjacent cages, $\mathrm{cov}(n_1, n_2)$, reveals the mechanism behind the cooperative adsorption exhibited in the adsorption isotherm in Fig. 2.

More generally, the covariance of the occupancy of cage i with the occupancy of a cage a distance k away is

$$\mathrm{cov}(n_i, n_{i+k}) := \langle n_i n_{i+k}\rangle - \langle n_i\rangle\langle n_{i+k}\rangle, \quad [11]$$

with the restriction $k \leq M/2$. In a Langmuir adsorption model, where each adsorption site behaves independently of the others, $\langle n_i n_{i+k}\rangle$ is independent of both i and k, and $\mathrm{cov}(n_1, n_2) = 0$ (*SI Appendix*, section S5.1). A positive $\mathrm{cov}(n_i, n_{i+k})$ indicates that the presence of an adsorbate a distance k from site i enhances the probability that site i is also occupied (*SI Appendix*, section S5.2); that is, $\mathrm{cov}(n_1, n_2) > 0$ implies cooperative adsorption and the tendency for adsorbates to spatially cluster. In *SI Appendix*, section S5, we derive an expression for $\mathrm{cov}(n_i, n_{i+k})$ in terms of the transfer matrix $\mathbf{P}$.

Fig. 3 displays the covariance of the occupancy of two adjacent cages, $\mathrm{cov}(n_1, n_2)$, in our model as a function of expected occupancy. The positive $\mathrm{cov}(n_1, n_2)$ implies cooperative adsorption. To understand the nature of the cooperativity, consider our system with n fixed [the canonical (NVT) ensemble]. In the most probable microstates for $n = 2$, the two adsorbates are in adjacent cages because this allows them to cooperate in incentivizing their shared ligand to rotate into the pore to achieve a greater guest–host interaction. From a different perspective, consider $n = 1$. The ligands on the faces of the occupied cage have a higher propensity to rotate into the pores than a ligand shared by two empty cages. Thus, the next gas molecule is more likely to adsorb in one of the two cages directly adjacent to the occupied cage than in another cage due to the more favorable interaction with a ligand that is rotated into the pores.

At both zero and full occupancy, $\mathrm{cov}(n_1, n_2)$ approaches zero; it peaks at half-fractional occupancy, exhibiting a symmetry. Consider when all cages are empty except cage 2. Per the argument above, for the next guest molecule, cage 1 and cage 3 are more favorable adsorption sites than the other empty cages. Although the additional molecule is thus more likely to adsorb in cage 1 or 3 than in any one of the other empty cages, the entropic incentive for the second adsorbate to explore the other $M - 3$ empty cages, despite their less favorable adsorption energy, renders $\mathrm{cov}(n_1, n_2)$ to be small when $n = 1$. To explain the symmetry, at the other extreme, considering a material with only one empty cage, entropy incentivizes a vacancy to explore all cages.

Conditions for the Inflection Point. For not all parameter regimes does the adsorption isotherm in our model exhibit an inflection (*SI Appendix*, Fig. S1). In *SI Appendix*, section S7, we investigate which regimes of parameter space present an inflection in the adsorption isotherm. We find that, qualitatively, an inflection is absent when ϵ_ℓ is significantly greater than ϵ; the energy enhancement ϵ of a guest–ligand interaction is not large enough to compensate for the intrahost energetic penalty ϵ_ℓ for the ligand to rotate into the pores. This finding is consistent with the analysis of the covariance of the occupancy of neighboring cages in the previous section; the cooperative adsorption effect leads to a convex adsorption isotherm at low coverage through the incentivization of ligands to be rotated into the pores in the presence of adsorbed gas molecules.

The role of entropy is underscored by the presence of an inflection in the adsorption isotherm when the intrahost energy penalty for ligand rotation is zero. For $\epsilon_\ell = 0$, a ligand shared by two empty cages has no energetic preference for one rotational conformation over another; entropy dictates that it fluctuates between its two conformations with equal probability ($\langle \ell/M\rangle = 1/2$ for the empty lattice when $\epsilon_\ell = 0$ (*SI Appendix*, section S4.3). For a ligand shared by two occupied cages, the ligand–guest interaction enhancement now lowers the energy of the ligand in its rotated state to -2ϵ. Depending on the temperature and magnitude of 2ϵ, the energetic incentive for ligands to rotate into the pore as more gas adsorbs overcomes the entropic incentive for half to remain parallel to the cage walls, resulting in a gradual transition in the most likely rotational states of the ligands and an inflection. The inflections for $\epsilon_\ell = 0$ occur at small loadings, however (*SI Appendix*, Fig. S2).

Engineering and Design Applications. Our model lends insights into how we can exploit rotating ligands in porous crystals for pressure-swing adsorption processes.

Intrinsic heat management. When gas is charged into an adsorbent, the heat released upon adsorption raises the temperature of the adsorbent. This leads to capacity losses compared with isothermal charging, as less gas is adsorbed at higher temperatures. Similarly, during gas discharge, the adsorbent cools and holds onto the gas (58). It is thus important to mitigate temperature changes in the adsorbent during gas (dis)charging.

Materials with ligands that undergo conformation changes offer an advantage over rigid materials in that they can achieve a high guest–host interaction while mitigating the heat released upon adsorption. When a guest molecule adsorbs and concomitantly induces a conformation change in a ligand, a fraction of the energy released upon adsorption is consumed by the endothermic process ($\epsilon_\ell > 0$) of the ligand undergoing the conformation change. This phenomenon of intrinsic heat management (56) is beneficial for mitigating capacity losses due to temperature changes of the adsorbent in adsorption-based engineering processes.

We demonstrate intrinsic heat management in our model material by finding the contribution to Q_{st} made by the intrahost energy $U_h := \epsilon_\ell \ell$. As $U = U_h + U_{gh}$, where U_h and U_{gh} are the first and second terms in Eq. **1**, respectively, the contribution to Q_{st} by the intrahost energy is

$$-\frac{\langle U_h n\rangle - \langle U_h\rangle\langle n\rangle}{\langle n^2\rangle - \langle n\rangle^2}, \quad [12]$$

which we show in Fig. 2 as the purple curve. As the contribution to Q_{st} by the rotatable moieties integrated into the host through U_h is negative, this demonstrates that the dynamic moieties in our model material serve to mitigate the heat of adsorption while, from the perspective of the adsorbate, retaining a high energy of adsorption to recruit guest molecules into the cages.

Engineering inflection points to maximize working capacity. We can exploit the inflection induced into the adsorption isotherm in materials with rotating ligands to achieve a higher working capacity in a pressure-swing adsorption process than possible with a rigid, Langmuirian material. For a pressure swing between pressures P_H and P_L, the (isothermal) working capacity w of a material is the amount of gas adsorbed at pressure P_H minus that adsorbed at P_L:

$$w(P_H, P_L) := \langle n\rangle(P_H) - \langle n\rangle(P_L). \quad [13]$$

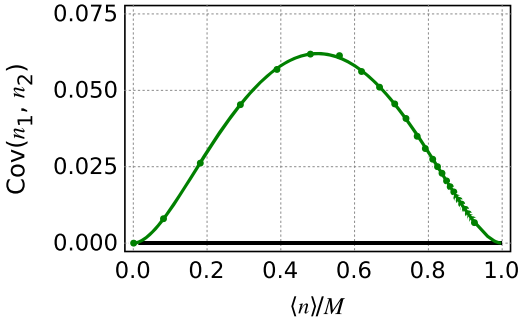

Fig. 3. Covariance of the occupancy of two neighboring cages cov(n_1, n_2) as a function of $\langle n\rangle/M$. Green curve is exact model solution. The horizontal, black line corresponds to a Langmuir adsorption model, where cov(n_1, n_2) = 0.

Consider a Langmuirian material with M adsorption cages with free volume V_0 and energy of adsorption ϵ_0, which is recovered by our model in the limit $\epsilon_\ell \to \infty$. Conceptually, the working capacity w is maximal for a particular ϵ_0: If the affinity of the adsorbate for the host is too weak (strong), the uptake will be too low at P_H (too high at P_L), resulting in a small working capacity (44, 45). The maximum achievable working capacity and corresponding energy of adsorption in a Langmuir model are (44, 45, 59)

$$w_{opt} := \max_{\epsilon_0} w(P_H, P_L) = M\left(\frac{\sqrt{P_H}-\sqrt{P_L}}{\sqrt{P_H}+\sqrt{P_L}}\right)$$

$$\epsilon_{0,opt} := \operatorname*{argmax}_{\epsilon_0} w(P_H, P_L) = k_B T \ln\left(\frac{\sqrt{P_L P_H}}{k_B T} V_0\right). \quad \textbf{[14]}$$

The maximum achievable working capacity w_{opt} for a rigid, Langmuirian material depends only on the number of adsorption sites M and the operating pressures, P_H and P_L. The black curve in Fig. 4 is an optimally shaped Langmuir adsorption isotherm obtained by tuning the energy of adsorption to $\epsilon_{0,opt}$ in Eq. **14**, using $P_H = 1.5$ bar, $P_L = 0.1$ bar for illustration.

We find the optimal energy of adsorption ϵ_0 in our model ($\epsilon, \epsilon_\ell, V_0, M$ fixed) by enforcing $\frac{\partial w}{\partial \epsilon_0} = 0$. Our model adsorption isotherm with the optimal ϵ_0 is the green curve in Fig. 4. Our optimally tuned model has a higher uptake at P_H and a lower uptake at P_L than the optimally tuned Langmuirian material with equal V_0 and M; both effects improve upon the working capacity of a Langmuirian material. We achieve a higher working capacity than the Langmuir model by using a smaller ϵ_0. The reason that a material with rotating ligands can achieve a higher working capacity than a rigid, Langmuirian model is revealed by again considering the extreme cases where adsorption is governed by Eq. **2**. At pressure P_L, when occupancy is low, the gas sees an adsorbent with energy of adsorption closer to ϵ_0. At pressure P_H, the higher occupancy will induce more ligands to rotate into the pores, and consequently the gas sees an adsorbent with energy of adsorption closer to $\epsilon_0 + 2\epsilon$. By using a smaller ϵ_0 than optimal for a Langmuir model in Eq. **14**, we mitigate uptake at P_L and rely on the ligands that rotate into the pores to recruit adsorbates into the pores at P_H through the enhancement of the guest–ligand interaction (ϵ).

We show how the optimal working capacity w_{opt} and corresponding $\epsilon_{0,opt}$ depend on the parameters ϵ_ℓ and ϵ in *SI Appendix*, Fig. S3. At $\epsilon = 0$, we recover the optimal parameters for a Langmuir model in Eq. **14**. For all $\epsilon, \epsilon_\ell > 0$, we achieve a higher optimal working capacity with our model than with a Langmuir model. For fixed ϵ, the working capacity is maximal for $\epsilon_\ell \approx \epsilon$, in line with our previous discussion that, for an inflection in the adsorption isotherm to occur, the intrahost energetic penalty for a ligand to rotate ϵ_ℓ must be comparable to the resulting guest–ligand energetic benefit ϵ. Interestingly, $\epsilon_{0,opt} < 0$ when ϵ is large and ϵ_ℓ is small; i.e., it is optimal in this region of parameter space for adsorption in a cage with both ligands unrotated to be energetically unfavorable to inhibit uptake at P_L, relying on the high affinity of a guest for a rotated ligand to recruit adsorbates at P_H. This resembles gate-opening behavior (60), although expansion work is also involved in gate opening (47).

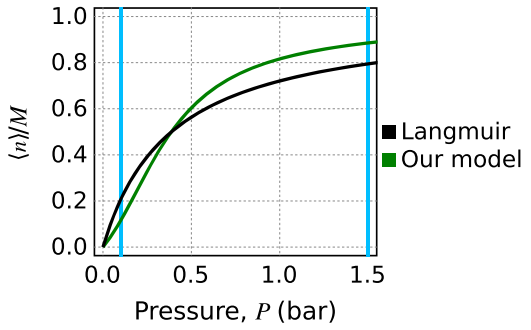

Fig. 4. Optimizing the working capacity for a pressure-swing adsorption process between $P_H = 1.5$ bar and $P_L = 0.1$ bar. We tuned ϵ_0 to optimize the working capacity in Eq. **13** for a Langmuir model (black) and our model material (green) with the same V_0 and M (ϵ_ℓ, ϵ fixed). Pressures P_H and P_L are shown as vertical, blue lines. The resulting $\epsilon_{0,opt} = 12.8$ kJ/mol for our model and 20.4 kJ/mol for the Langmuir model.

Mean-Field Approximation. The model in Fig. 1 is quasi-one dimensional in that each adsorption cage is coupled to only two neighboring cages through its shared ligands. We now find a mean-field solution of our model, which we expect to approximate the behavior of a d-dimensional model (with the approximation improving with increasing d), where each adsorption cage is coupled to neighbors in $d \geq 2$ dimensions through $2d$ shared, rotating ligands on its faces (*SI Appendix*, Fig. S11). In addition, the mean-field model provides more insights into the behavior of our system than the exact solution because it results in simpler and thus more interpretable expressions for the adsorption isotherm and concomitant ligand configurations.

The internal energy in Eq. **1** cannot be written as $U(n, \ell)$ because it depends on the precise arrangement of the n adsorbates in the M cages and precisely which ℓ of the Md ligands have undergone a conformation change. Here, we approximate U by treating the interaction between adsorbates and ligands with a mean field of ligands. The internal energy of our system under the mean-field approximation, $U_{mf}(n, \ell)$, is

$$U_{mf}(n, \ell) = \epsilon_\ell \ell - n\left(\epsilon_0 + 2d\epsilon\frac{\ell}{Md}\right), \quad \textbf{[15]}$$

because each adsorbed molecule sees a mean field of $2d[\ell/(Md)]$ ligands protruding into the pore; $\ell/(Md)$ is the probability that a given ligand is rotated into the pore given no information about which n of the M cages are occupied.

Our approach in solving the mean-field model in the grand-canonical ensemble is to write an expression for the grand potential, Ω, of the system,

$$\Omega(\mu, M, \beta) := U - TS - \mu n, \quad \textbf{[16]}$$

and analyze its derivatives because, at thermodynamic equilibrium, the grand potential of the system is minimized in the grand-canonical ensemble. The internal energy U for constructing Ω_{mf} is given by Eq. **15**. We directly write the entropy S of the system by counting the microstates that exhibit n adsorbed molecules and ℓ rotated ligands and accounting for the translational entropy of each adsorbed particle in its cage. We arrive at

$$\Omega_{mf}(\mu, M, \beta) = \epsilon_\ell \ell - n\left(\epsilon_0 + 2\epsilon\frac{\ell}{M}\right) - k_B T \log\left(\binom{M}{n}\binom{Md}{\ell}(\Lambda^{-3} V_0)^n\right) - \mu n. \quad \textbf{[17]}$$

Eq. **17** can be partitioned into the sum of the free energy of the host, the free energy of the adsorbed molecules, and the chemical potential term. We now proceed to find the self-consistency equations, where we apply Stirling's approximation to the factorial terms.

Self-consistency equation for ℓ. At thermodynamic equilibrium, the ligands will adopt microstates that minimize the grand potential of the system,

$$\left(\frac{\partial \Omega_{mf}}{\partial \ell}\right)_{\beta\mu,\,\beta,\,M} = 0, \qquad [18]$$

leading to the self-consistency equation for ℓ,

$$\frac{\ell}{Md} = \frac{1}{1+e^{\beta(\epsilon_\ell - 2\epsilon n/M)}}. \qquad [19]$$

For fixed n, we arrive at a simple two-level system, where each ligand fluctuates between two energy states that differ in energy by $\epsilon_\ell - 2\epsilon n/M$.

When the cages are empty ($n = 0$), the fraction of ligands protruding into the pores goes to zero as the energetic penalty for ligand rotation increases ($\epsilon_\ell \to \infty$) and goes to the entropically favored $\frac{1}{2}$ when the host has no energetic preference for one ligand configuration over another ($\epsilon_\ell = 0$). As gas adsorbs (n/M increases), the energetic benefit of a protruding ligand to the gas molecules diminishes the intrahost energetic penalty for ligand rotation, resulting in a greater fraction of ligands rotating into the pore. If $2\epsilon > \epsilon_\ell$, the sign in the exponent in Eq. **19** changes at some occupancy, and thus the temperature dependence of the ligand configurations qualitatively changes: At low occupancy, entropically driven fluctuations have the effect of increasing the number of ligands rotated into the pores, whereas at high occupancies, they increase the number of ligands aligned with the cage walls. This is because the ligand configuration that minimizes the internal energy of the system switches at a given value of n under the condition $2\epsilon > \epsilon_\ell$ (Eq. **15**). This switching of ligand temperature dependence arises in the exact solution also (*SI Appendix*, section S4.4).

Self-consistency equation for n. At thermodynamic equilibrium, the number of adsorbed molecules is dictated by the minimum of the grand potential of the system:

$$\left(\frac{\partial \Omega_{mf}}{\partial n}\right)_{\beta\mu,\,\beta,\,M} = 0. \qquad [20]$$

This leads to the self-consistency condition for n:

$$\frac{n}{M} = \frac{e^{\beta(\epsilon_0 + 2\epsilon\ell/M)} V_0 \beta P}{1 + e^{\beta(\epsilon_0 + 2\epsilon\ell/M)} V_0 \beta P}. \qquad [21]$$

The adsorption isotherm under mean-field theory takes the character of a Langmuir adsorption isotherm with a Langmuir parameter $K := \beta V_0 e^{\beta(\epsilon_0 + 2\epsilon\ell/M)}$ that is a function of the fraction of ligands rotated into the pores, $\ell/(Md)$. As $\ell/(Md)$ increases, the Langmuir parameter increases due to the greater affinity of the host for the guest when the ligands are rotated into the pores.

Mean-field solution. The mean-field solution to the model is then described by the coupled Eqs. **19** and **21**. We can solve these equations graphically by plotting them in the (n, ℓ) plane. The red curve in Fig. 5*A* displays Eq. **19**, which is independent of pressure, whereas the series of blue curves show Eq. **21** for different pressures. The intersection of the red and blue curves dictates the solution at that particular pressure. We observe a first-order phase transition. At low pressures, only one solution at low n and ℓ exists. As we increase the pressure, a saddle node bifurcation (61) occurs, where a stable solution at high n and ℓ suddenly appears in addition to the low-n solution. Eventually, at higher pressure, the low-n solution suddenly disappears. This result could yield adsorption–desorption hysteresis. From another perspective, the grand potential Ω_{mf} is bistable at intermediate pressures (*SI Appendix*, Fig. S4), much like the bistable osmotic potential that explains hysteretic breathing transitions in MOFs (49, 50, 62).

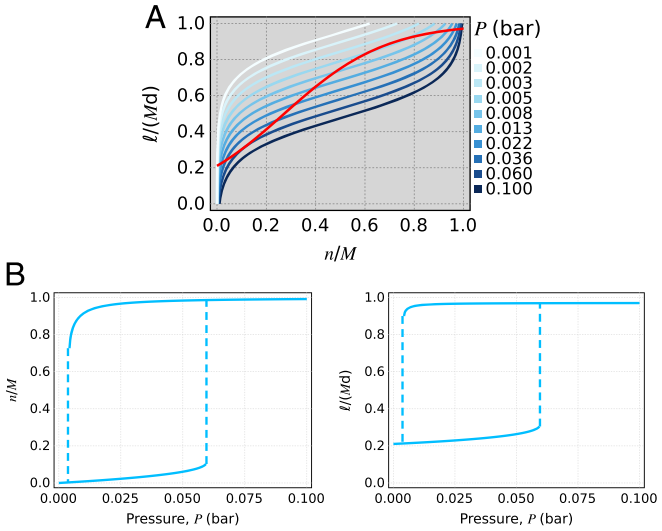

Fig. 5. Mean-field theory solution for $d = 2$. (*A*) Graphical solution to mean-field theory self-consistency Eqs. **19** and **21**. The red curve shows Eq. **19**, which is independent of pressure. The series of blue curves show Eq. **21** for different pressures. The intersection of a blue curve with the red curve is the mean-field theory solution for a given pressure. (*B*) The adsorption isotherm (*Left*) and ligand configurations (*Right*) according to mean-field theory. The dashed lines show the adsorption–desorption hysteresis loop that could arise.

Fig. 5*B* shows the adsorption isotherm and corresponding ligand configurations for the mean-field model. In contrast to the exact solution in Fig. 2, where a smooth inflection is present in the adsorption isotherm as the ligands gradually rotate into the pores, we see discontinuous jumps in the adsorption isotherm and concomitant ligand configurations under the mean-field model approximation in conjunction with the bifurcations in Fig. 5*A*. At intermediate pressures, there are two solutions, as Fig. 5*A* shows. Depending on the magnitude of the fluctuations, this could manifest as an adsorption–desorption hysteresis loop.

Thus, when cages are coupled together by shared ligands in multiple dimensions, these rotating ligands can (*i*) induce abrupt steps in adsorption isotherms and (*ii*) yield adsorption–desorption hysteresis loops. Both of these features are not found in the quasi–one-dimensional model. In *SI Appendix*, section S13, we use Monte Carlo simulations to study a 2D variant of our model and indeed find evidence of a first-order phase transition as the mean-field theory predicts, albeit at a lower temperature as expected due to the overestimation of the critical temperature by mean-field theory in its neglect of fluctuations.

Case Study: MIL-91(Al)

We consider MIL-91(Al) (63) as a case study. The activated MIL-91(Al) crystal structure in vacuum is shown in Fig. 6*A*. Llewellyn et al. (30) conducted in situ X-ray powder diffraction (XRPD) experiments and found that the ligands in MIL-91(Al), when loaded with CO_2 gas, twist by $\sim 20^\circ$ (compare Fig. 6 *A* and *B*). MIL-91(Al) maintains its topology, and its unit cell volume increases less than 4% when loaded with CO_2. The authors observed an inflection in the CO_2 adsorption isotherm in MIL-91(Al) at 303 K (*SI Appendix*, Fig. S5). Molecular simulations of CO_2 adsorption in the two rigid-host conformers, analogous to the red and blue curves in Fig. 2, supported that the inflection is a consequence of the twisting ligands. The in situ XRPD experiments at varying CO_2 loadings showed a gradual change in a peak attributed to the Al-OH-Al angle, suggesting that the structure changes its conformation gradually.

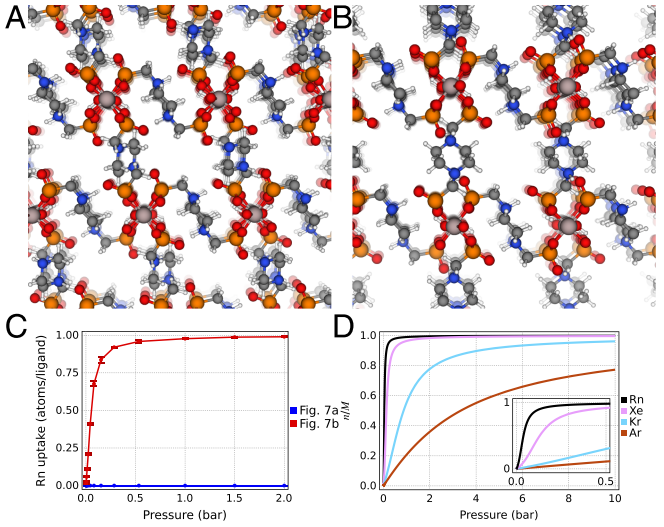

Fig. 6. MIL-91(Al) case study. (*A* and *B*) MIL-91(Al) crystal structures in vacuum (*A*) and when loaded with CO_2 gas (*B*). These are DFT energy-minimized structures using empty and CO_2-loaded structures from ref. 30 as starting points. (light gray, Al; dark gray, C; white, H; blue, N; red, O; orange, P). (*C*) Simulated Rn adsorption isotherms at 298 K in the rigid hosts depicted in *A* (blue) and in *B* (red). (*D*) Model predictions for Rn, Xe, Kr, and Ar adsorption isotherms in MIL-91(Al) at 298 K. *Inset* shows a rescaling of the pressure axis to see the inflections in the Xe and Rn adsorption isotherms.

We used density functional theory (DFT) calculations (*SI Appendix*, section S11.1) to find the energy-minimized MIL-91(Al) structure(s) using the experimentally reported (30) empty and CO_2-loaded structures (without the CO_2) as starting points. The DFT calculations capture the bistability of MIL-91(Al); the minimizations converged to two distinct conformers. According to our DFT calculations, the conformation in Fig. 6*A* is more stable by 3 kJ/mol of twisting ligands. Thus, in the context of our model, we identify $\epsilon_\ell = 3$ kJ/mol for MIL-91(Al).

As more than one CO_2 molecule can adsorb per ligand in MIL-91(Al) (30), radon adsorption in MIL-91(Al) fits better into the context of our model because only one atom per ligand can fit into its pores. Fig. 6*C* displays the simulated rigid-host Rn adsorption isotherms in the two conformers of MIL-91(Al). See *SI Appendix*, section S11 for methods. In the more stable conformer, the adsorption is negligible because an adsorbed Rn experiences steric hindrance. On the other hand, Rn adsorbs favorably in the less stable conformer in Fig. 6*B*. The other noble gases, xenon, krypton, and argon also exhibit a one-atom per ligand saturation loading in MIL-91(Al) and adsorb more favorably in the conformer in Fig. 6*B* (*SI Appendix*, Fig. S6).

Rn, Xe, Kr, and Ar adsorption in MIL-91(Al) thus may fit into the context of our model because (*i*) the adsorbate–host interaction is greater when the ligands twist, yet intrahost forces penalize ligand twisting; (*ii*) the ligands are shared between cages in a quasi–one-dimensional manner (*SI Appendix*, Fig. S7); (*iii*) maximally only one atom adsorbs per ligand; (*iv*) as the CO_2 adsorption and XRPD data show gradual changes, each ligand can likely adopt one of its two rotational conformations independently of the other ligands [alternatively, we can model layers/sheets of ligands twisting simultaneously as in the model for MIL-53 breathing by Triguero et al. (48)]. We identified the ϵ_0, ϵ, and V_0 parameters that model Rn, Xe, Kr, and Ar adsorption in MIL-91(Al) from the simulated energy of adsorption in the two conformers in Fig. 6 *A* and *B* and pore volume calculations. Fig. 6*D* shows the predicted adsorption isotherms of Rn, Xe, Kr, and Ar in MIL-91(Al) by our model, using our estimates of ϵ_0, ϵ, and V_0 for each adsorbate. The model predicts a noticeable inflection in the Rn, Xe, and Kr adsorption isotherms in MIL-91(Al), but not in Ar, as the energetic enhancement ϵ due to ligand rotation is rather small for Ar (2.5 kJ/mol). As expected, the ranking of adsorption follows the size of the noble gas atom.

Discussion

We posed and solved a statistical mechanical model of gas adsorption in a porous material whose cages share a flexible ligand that can adopt two distinct rotational conformations. An affinity of the gas molecule for the ligand incentivizes the ligand to undergo a conformation change, but intrahost forces impose an energetic penalty for doing so. We showed that these two competing forces can give rise to an inflection in the adsorption isotherm as the gas gradually changes the set of most probable conformations that the adsorbent adopts to achieve a greater guest–host interaction. We demonstrated that cooperative adsorption arises from the coupling of neighboring sites through their shared ligand; when a gas molecule adsorbs and induces a ligand to change its rotational conformation, it enhances the favorability for adsorption in the neighboring cage that shares that ligand, facilitating the recruitment of an additional adsorbate. When adsorption cages are coupled together by rotating ligands in higher dimensions, our mean-field solution showed that abrupt steps in the adsorption isotherm and adsorption–desorption hysteresis can occur.

We proved that porous materials whose cages share rotating ligands can achieve a greater working capacity in a pressure-swing adsorption process than a rigid, Langmuirian material. Our model informed that the working capacity is maximized when the enhancement of the guest–ligand affinity upon ligand rotation is of the same order as the intrahost penalty for the ligand to rotate. As an additional benefit, the endothermic conformation change of a ligand intrinsically mitigates temperature changes of the adsorbent when gas (de-)adsorbs.

Our model is generalizable in that a ligand rotation represents a conformational change of some flexible constituent integrated into the MOF that exposes a more favorable binding site for a guest molecule on both sides of the cage wall.

The cages of many porous materials with rotating ligands can fit more than one adsorbate molecule. In *SI Appendix*, section S12, we consider the case where multiple adsorbate molecules can fit in a cage with rotating ligands on each side. Cooperative adsorption still arises due to the coupling of the two adsorption sites that do share a ligand. Adsorbate–adsorbate attractions enhance this cooperativity by transmitting a ligand's influence across longer length scales.

In our model, the ligands change conformation to achieve a more favorable guest–host interaction. We duly note that a conformational change could also be driven by entropy or chemical potential (Eq. **16**); i.e., ligands could rotate to afford the guest molecule more translation and/or rotational degrees of freedom or to create a larger pore to accommodate more molecules. For example, the MOF in ref. 18 persists in a narrow-pore form in the absence of adsorbed CO_2 molecules. Upon adsorbing a given amount of CO_2, the pyridyl rings in the MOF rotate, yielding a larger pore that can accommodate more CO_2 molecules. The intuition gained from our model is still applicable here: The adsorbent transitions from the narrow-pore form preferred in the absence of gas molecules to the large-pore form when enough gas adsorbs, causing an inflection in the adsorption isotherm.

Note that adsorption isotherms in rigid materials can exhibit inflections as well, through mechanisms such as pore filling (64), strong adsorbate–adsorbate attractions [the quadratic adsorption isotherm (65)] (66), and commensurate-to-incommensurate adsorption transitions (67).

Future work remains. One direction entails investigating the behavior of our model in the presence of gas mixtures. Akin to how protein flexibility in the induced-fit and conformational

selection models (20, 21) for enzyme–substrate binding plays a crucial role in the recognition of biological molecules and selectivity of enzymes, flexible moieties in MOFs may enhance their selectivity for gas separations, catalysis, and chemical sensing. In *SI Appendix*, section S14, we show that the rotating ligands in our model material could enhance the selectivity over that of a rigid counterpart via differing ligand–adsorbate interaction enhancements (ϵ).

Further modeling could reveal interesting behavior arising from features involved in other reported MOFs with dynamic constituents, such as the MOF of Seo et al. (29), where rotating ligands reach across the cage to interact with each other. Such different paradigms of moving constituents in porous materials likely need to be built into a specialized model and studied on a case-by-case basis. Another direction for future work is to include in our model external stimuli to modulate the ligand conformations and thus, indirectly, the host–guest interaction. For example, spin crossover transitions of a metal in a MOF (68) have been shown to modulate the rotational freedom of coordinating ligands (69), opening an avenue for switching the ligand state with an electric field, temperature, or light (70). For asymmetric ligands with polar groups, an electric field could modulate the rotational conformations (71, 72).

Because flexibility can influence diffusion (73), another follow-up study is to investigate the impact of a rotating ligand on molecular diffusion. As an adsorbate molecule percolates through the pores of a MOF with a rotating ligand, ligands may need to concomitantly rotate, much like a turnstile, which will influence diffusion.

ACKNOWLEDGMENTS. We thank Guillaume Maurin for discussions and MIL-91(Al) crystal structures. C.M.S. and E.B., who performed the research, are supported by the Center for Gas Separations Relevant to Clean Energy Technologies, an Energy Frontier Research Center funded by the US Department of Energy (DOE), Office of Basic Energy Sciences under Award DE-SC0001015. C.C. gratefully acknowledges partial support from the National Science Foundation Sustainable Chemistry, Engineering, and Materials (SusChEM) initiative under Grant DMR 1410557. The research of B.S. has received funding from the European Research Council under the European Union's Horizon 2020 research and innovation program (Grant 666983, MaGic). This research used resources of the National Energy Research Scientific Computing Center, a DOE Office of Science User Facility supported by the Office of Science of the US DOE under Contract DE-AC02-05CH11231.

1. Zhou HC, Long JR, Yaghi OM (2012) Introduction to metal–organic frameworks. *Chem Rev* 112(2):673–674.
2. Schoedel A, Ji Z, Yaghi OM (2016) The role of metal–organic frameworks in a carbon-neutral energy cycle. *Nat Energy* 1:16034.
3. Morris RE, Wheatley PS (2008) Gas storage in nanoporous materials. *Angew Chem Int Ed Engl* 47(27):4966–4981.
4. Li JR, Kuppler RJ, Zhou HC (2009) Selective gas adsorption and separation in metal–organic frameworks. *Chem Soc Rev* 38(5):1477–1504.
5. Kreno LE, et al. (2012) Metal–organic framework materials as chemical sensors. *Chem Rev* 112(2):1105–1125.
6. Horcajada P, et al. (2008) Flexible porous metal-organic frameworks for a controlled drug delivery. *J Am Chem Soc* 130(21):6774–6780.
7. Lee J, et al. (2009) Metal–organic framework materials as catalysts. *Chem Soc Rev* 38(5):1450–1459.
8. Yaghi OM, et al. (2003) Reticular synthesis and the design of new materials. *Nature* 423(6941):705–714.
9. Furukawa H, Cordova KE, O'Keeffe M, Yaghi OM (2013) The chemistry and applications of metal-organic frameworks. *Science* 341(6149):1230444.
10. Fletcher AJ, Thomas KM, Rosseinsky MJ (2005) Flexibility in metal-organic framework materials: Impact on sorption properties. *J Solid State Chem* 178(8):2491–2510.
11. Horike S, Shimomura S, Kitagawa S (2009) Soft porous crystals. *Nat Chem* 1(9):695–704.
12. Schneemann A, et al. (2014) Flexible metal–organic frameworks. *Chem Soc Rev* 43(16):6062–6096.
13. Coudert FX (2015) Responsive metal–organic frameworks and framework materials: Under pressure, taking the heat, in the spotlight, with friends. *Chem Mater* 27(6):190–1916.
14. Férey G, Serre C (2009) Large breathing effects in three-dimensional porous hybrid matter: Facts, analyses, rules and consequences. *Chem Soc Rev* 38(5):1380–1399.
15. Serre C, et al. (2002) Very large breathing effect in the first nanoporous chromium (III)-based solids: MIL-53 or Cr^{III} $(OH)\cdot\{O_2C\text{-}C_6H_4\text{-}CO_2\}\cdot\{HO_2C\text{-}C_6H_4\text{-}CO_2H\}_x\cdot H_2O_y$. *J Am Chem Soc* 124(45):13519–13526.
16. Serre C, et al. (2007) Role of solvent-host interactions that lead to very large swelling of hybrid frameworks. *Science* 315(5820):1828–1831.
17. Kitaura R, Seki K, Akiyama G, Kitagawa S (2003) Porous coordination-polymer crystals with gated channels specific for supercritical gases. *Angew Chem Int Ed Engl* 42(4):428–431.
18. Yang W, et al. (2012) Selective CO_2 uptake and inverse CO_2/C_2H_2 selectivity in a dynamic bifunctional metal-organic framework. *Chem Sci* 3(10):2993–2999.
19. Dybtsev DN, Chun H, Kim K (2004) Rigid and flexible: A highly porous metal–organic framework with unusual guest-dependent dynamic behavior. *Angew Chem* 116(38):5143–5146.
20. Koshland DE (1995) The key–lock theory and the induced fit theory. *Angew Chem Int Ed Engl* 33(2324):2375–2378.
21. Boehr DD, Nussinov R, Wright PE (2009) The role of dynamic conformational ensembles in biomolecular recognition. *Nat Chem Biol* 5(11):789–796.
22. Balzani VV, Credi A, Raymo FM, Stoddart JF (2000) Artificial molecular machines. *Angew Chem Int Ed Engl* 39(19):3348–3391.
23. Zhu K, O'Keefe CA, Vukotic VN, Schurko RW, Loeb SJ (2015) A molecular shuttle that operates inside a metal–organic framework. *Nat Chem* 7(6):514–519.
24. Horike S, et al. (2006) Dynamic motion of building blocks in porous coordination polymers. *Angew Chem Int Ed Engl* 45(43):7226–7230.
25. Kubota Y, et al. (2006) Metastable sorption state of a metal–organic porous material determined by in situ synchrotron powder diffraction. *Angew Chem* 118(30):5054–5058.
26. Gould SL, Tranchemontagne D, Yaghi OM, Garcia-Garibay MA (2008) Amphidynamic character of crystalline MOF-5: Rotational dynamics of terephthalate phenylenes in a free-volume, sterically unhindered environment. *J Am Chem Soc* 130(11):3246–3247.
27. Morris W, Taylor RE, Dybowski C, Yaghi OM, Garcia-Garibay MA (2011) Framework mobility in the metal–organic framework crystal IRMOF-3: Evidence for aromatic ring and amine rotation. *J Mol Struct* 1004(1-3):94–101.
28. Fairen-Jimenez D, et al. (2011) Opening the gate: Framework flexibility in ZIF-8 explored by experiments and simulations. *J Am Chem Soc* 133(23):8900–8902.
29. Seo J, Matsuda R, Sakamoto H, Bonneau C, Kitagawa S (2009) A pillared-layer coordination polymer with a rotatable pillar acting as a molecular gate for guest molecules. *J Am Chem Soc* 131(35):12792–12800.
30. Llewellyn PL, et al. (2015) Structural origin of unusual CO_2 adsorption behavior of a small-pore aluminum bisphosphonate MOF. *J Phys Chem C* 119(8):4208–4216.
31. Lin ZJ, Lü J, Hong M, Cao R (2014) Metal–organic frameworks based on flexible ligands (FL-MOFs): Structures and applications. *Chem Soc Rev* 43(16):5867–5895.
32. Inukai M, et al. (2015) Control of molecular rotor rotational frequencies in porous coordination polymers using a solid-solution approach. *J Am Chem Soc* 137(38):12183–12186.
33. Banerjee D, et al. (2016) Direct structural identification of gas induced gate-opening coupled with commensurate adsorption in a microporous metal–organic framework. *Chemistry* 22(33):11816–11825.
34. Burtch NC, et al. (2015) Understanding DABCO nanorotor dynamics in isostructural metal–organic frameworks. *J Phys Chem Lett* 6(5):812–816.
35. Kolokolov DI, et al. (2010) Dynamics of benzene rings in MIL-53 (Cr) and MIL-47 (V) frameworks studied by 2H NMR spectroscopy. *Angew Chem Int Ed Engl* 49(28):4791–4794.
36. Kottas GS, Clarke LI, Horinek D, Michl J (2005) Artificial molecular rotors. *Chem Rev* 105(4):1281–1376.
37. Murdock CR, McNutt NW, Keffer DJ, Jenkins DM (2014) Rotating phenyl rings as a guest-dependent switch in two-dimensional metal–organic frameworks. *J Am Chem Soc* 136(2):671–678.
38. Hughes BC, Murdock CR, Jenkins DM (2015) Isoreticular synthesis of 2D MOFs with rotating aryl rings. *Inorg Chem Front* 2(11):1001–1005.
39. Gücüyener C, van den Bergh J, Gascon J, Kapteijn F (2010) Ethane/ethene separation turned on its head: Selective ethane adsorption on the metal–organic framework ZIF-7 through a gate-opening mechanism. *J Am Chem Soc* 132(50):17704–17706.
40. Aguado S, et al. (2011) Guest-induced gate-opening of a zeolite imidazolate framework. *New J Chem* 35(3):546–550.
41. Uemura K, Yamasaki Y, Komagawa Y, Tanaka K, Kita H (2007) Two-step adsorption/desorption on a jungle-gym-type porous coordination polymer. *Angew Chem* 119(35):6782–6785.
42. Krause S, et al. (2016) A pressure-amplifying framework material with negative gas adsorption transitions. *Nature* 532(7599):348–352.
43. Hyun SM, et al. (2016) Exploration of gate-opening and breathing phenomena in a tailored flexible metal–organic framework. *Inorg Chem* 55(4):1920–1925.
44. Bhatia SK, Myers AL (2006) Optimum conditions for adsorptive storage. *Langmuir* 22(4):1688–1700.
45. Simon CM, et al. (2014) Optimizing nanoporous materials for gas storage. *Phys Chem Chem Phys* 16:5499–5513.
46. Chang KJ, Talu O (1996) Behavior and performance of adsorptive natural gas storage cylinders during discharge. *Appl Therm Eng* 16(5):359–374.
47. Coudert FX, Jeffroy M, Fuchs AH, Boutin A, Mellot-Draznieks C (2008) Thermodynamics of guest-induced structural transitions in hybrid organic-inorganic frameworks. *J Am Chem Soc* 130(43):14294–14302.
48. Triguero C, Coudert FX, Boutin A, Fuchs AH, Neimark AV (2011) Mechanism of breathing transitions in metal–organic frameworks. *J Phys Chem Lett* 2(16):2033–2037.
49. Bousquet D, et al. (2013) Adsorption induced transitions in soft porous crystals: An osmotic potential approach to multistability and intermediate structures. *J Chem Phys* 138(17):174706.
50. Ghysels A, et al. (2013) On the thermodynamics of framework breathing: A free energy model for gas adsorption in MIL-53. *J Phys Chem C* 117(22):11540–11554.

51. Dunne LJ, Manos G (2016) Exact matrix treatment of an osmotic ensemble model of adsorption and pressure induced structural transitions in metal organic frameworks. *Dalton Trans* 45(10):4213–4217.
52. Shell MS (2015) *Thermodynamics and Statistical Mechanics: An Integrated Approach* (Cambridge Univ Press).
53. Sircar S, Mohr R, Ristic C, Rao MB (1999) Isosteric heat of adsorption: Theory and experiment. *J Phys Chem B* 103(31):6539–6546.
54. Geier SJ, et al. (2013) Selective adsorption of ethylene over ethane and propylene over propane in the metal–organic frameworks M_2(dobdc)(M = Mg, Mn, Fe, Co, Ni, Zn). *Chem Sci* 4(5):2054–2061.
55. Hulvey Z, et al. (2013) Noble gas adsorption in copper trimesate, HKUST-1: An experimental and computational study. *J Phys Chem C* 117(39):20116–20126.
56. Mason JA, et al. (2015) Methane storage in flexible metal–organic frameworks with intrinsic thermal management. *Nature* 527(7578):357–361.
57. Karavias F, Myers AL (1991) Isosteric heats of multicomponent adsorption: Thermodynamics and computer simulations. *Langmuir* 7(12):3118–3126.
58. Chang KJ, Talu O (1996) Behavior and performance of adsorptive natural gas storage cylinders during discharge. *Appl Therm Eng* 16(5):359–374.
59. Matranga KR, Myers AL, Glandt ED (1992) Storage of natural gas by adsorption on activated carbon. *Chem Eng Sci* 47(7):1569–1579.
60. Li D, Kaneko K (2001) Hydrogen bond-regulated microporous nature of copper complex-assembled microcrystals. *Chem Phys Lett* 335(1-2):50–56.
61. Strogatz SH (2014) *Nonlinear Dynamics and Chaos: With Applications to Physics, Biology, Chemistry, and Engineering* (Westview).
62. Bousquet D, Coudert FX, Boutin A (2012) Free energy landscapes for the thermodynamic understanding of adsorption-induced deformations and structural transitions in porous materials. *J Chem Phys* 137(4):044118.
63. Serre C, et al. (2006) Synthesis, structure and properties of related microporous N, N′-piperazinebismethylenephosphonates of aluminum and titanium. *Chem Mater* 18(6):1451–1457.
64. Walton KS, et al. (2008) Understanding inflections and steps in carbon dioxide adsorption isotherms in metal-organic frameworks. *J Am Chem Soc* 130(2): 406–407.
65. Hill TL (2012) *An Introduction to Statistical Thermodynamics* (Courier Corporation).
66. Moreau M, Valentin P, Vidal-Madjar C, Lin BC, Guiochon G (1991) Adsorption isotherm model for multicomponent adsorbate-adsorbate interactions. *J Colloid Interface Sci* 141(1):127–136.
67. Bak P (1982) Commensurate phases, incommensurate phases and the devil's staircase. *Rep Prog Phys* 45(6):587–629.
68. Ohba M, et al. (2009) Bidirectional chemo-switching of spin state in a microporous framework. *Angew Chem Int Ed Engl* 48(26):4767–4771.
69. Rodríguez-Velamazán JA, et al. (2012) A switchable molecular rotator: Neutron spectroscopy study on a polymeric spin-crossover compound. *J Am Chem Soc* 134(11):5083–5089.
70. Gütlich P, Garcia Y, Goodwin HA (2000) Spin crossover phenomena in Fe(II) complexes. *Chem Soc Rev* 29:419–427.
71. Devautour-Vinot S, et al. (2012) Structure and dynamics of the functionalized MOF type UiO-66 (Zr): NMR and dielectric relaxation spectroscopies coupled with DFT calculations. *Chem Mater* 24(11):2168–2177.
72. Winston EB, et al. (2008) Dipolar molecular rotors in the metal–organic framework crystal IRMOF-2. *Phys Chem Chem Phys* 10(34):5188–5191.
73. Haldoupis E, Watanabe T, Nair S, Sholl DS (2012) Quantifying large effects of framework flexibility on diffusion in MOFs: CH_4 and CO_2 in ZIF-8. *ChemPhysChem* 13(15):3449–3452.